American Mineralogist, Volume 77, pages 179–188, 1992

Geochemical alteration of pyrochlore group minerals: Microlite subgroup

GREGORY R. LUMPKIN
Advanced Materials Program, Australian Nuclear Science and Technology Organisation, Private Mail Bag 1, Menai, New South Wales 2234, Australia

RODNEY C. EWING
Department of Geology, University of New Mexico, Albuquerque, New Mexico 87131, U.S.A.

ABSTRACT

A qualitative picture of microlite stability is derived from known mineral assemblages and reactions in the simplified system Na-Ca-Mn-Ta-O-H. Results suggest that microlite is stable under conditions of moderate to high a_{Na^+} and $a_{Ca^{2+}}$ and low to moderate $a_{Mn^{2+}}$. Microlite is often replaced during the latter stages of granitic pegmatite evolution by manganotantalite and fersmite or rynersonite, indicating increasing $a_{Ca^{2+}}$ and $a_{Mn^{2+}}$ relative to a_{Na^+}. Primary (hydrothermal) alteration involves replacement of Na, F, and vacancies by Ca and O, represented by the coupled substitutions $^{A}Na^{Y}F \rightarrow {}^{A}Ca^{Y}O$ and $^{A}\square^{Y}\square \rightarrow {}^{A}Ca^{Y}O$. Exchange reactions between microlite and fluid suggest conditions of relatively high pH, high $a_{Ca^{2+}}$, low to moderate a_{HF}, and low a_{Na^+} during alteration by evolved pegmatite fluids at 350–550 °C and 2–4 kbar. Secondary (weathering) alteration involves leaching of Na, Ca, F, and O, represented by the coupled substitutions $^{A}Na^{Y}F \rightarrow {}^{A}\square^{Y}\square$, $^{A}Ca^{Y}O \rightarrow {}^{A}\square^{Y}\square$ and $^{A}Ca^{X}O \rightarrow {}^{A}\square^{X}\square$. Up to 80% of the A sites may be vacant, usually accompanied by a comparable number of anion (X + Y) vacancies and H_2O molecules. Secondary alteration results from interaction with relatively acidic meteoric H_2O at temperatures below 100 °C. In both types of alteration, the U content remains remarkably constant. Loss of radiogenic Pb due to long-term diffusion overprints changes in Pb content associated with primary alteration in most samples.

INTRODUCTION

Microlite, the Ta-rich member of the pyrochlore group (Hogarth, 1977), is largely restricted to evolved granitic pegmatites of the beryl-columbite, complex spodumene, and complex lepidolite types (Černý, 1989). The crystal structure is cubic ($Fd3m$, $Z = 8$), a derivative of the fluorite structure type, and has the general formula $A_{2-m}B_2X_{6-w}Y_{1-n}\cdot pH_2O$ (Lumpkin, 1989). End-member microlite has the ideal composition $NaCaTa_2O_6F$. A number of simple and coupled substitutions are possible, primarily involving Na, Ca, U, and vacancies at the A site; Ta, Nb, and Ti at the B site; and O, OH, F, and vacancies at the Y site (Lumpkin et al., 1986). The X site is normally fully occupied by O; however, small amounts of F and OH and vacancies may occur on the X site in natural samples (Lumpkin, 1989), consistent with previous work on synthetic pyrochlores (Groult et al., 1982; Rotella et al., 1982; Subramanian et al., 1983). Vacancies are tolerated mainly as defect components that can be written as $A_2B_2X_6\square$, $\square AB_2X_6\square$, and $\square_2B_2X_6M$ (Chakoumakos, 1984). In the latter case, the Y site is occupied by large monovalent cations like K, Rb, and Cs. The ability to accept a variety of elements, vacancies, and H_2O molecules suggests that microlite may be a useful indicator of relative changes in fluid composition in granitic pegmatites.

Alteration processes have been divided into primary and secondary types by Van Wambeke (1970) and Ewing (1975). Primary alteration is hydrothermal in nature and is usually associated with emplacement of the host rocks. This type of alteration is most likely to occur prior to significant radiation damage due to α decay of ^{238}U, ^{235}U, and ^{232}Th, resulting in either a change in composition or replacement by one or more phases. Secondary alteration is a near-surface phenomenon associated with weathering and often occurs after the crystal structure has been rendered fully aperiodic (metamict) by radiation damage. Secondary alteration leads to major increases in vacancies due to leaching of A-site cations and Y-site anions and to increased hydration (Van Wambeke, 1970; Ewing, 1975; von Knorring and Fadipe, 1981; Lumpkin and Ewing, 1985; Lumpkin et al., 1986).

This paper has four purposes: (1) to describe potential replacement reactions and chemical changes that accompany primary alteration, (2) to determine the maximum number of A-site vacancies resulting from secondary alteration along with any attending cation exchange effects, (3) to estimate the maximum number of anion vacancies and determine whether they correlate with cation vacancies; and (4) to outline the P-T-X conditions of alteration for the microlite subgroup in granitic pegmatites. Results of this study are also relevant to the disposal of nuclear waste in ceramic materials that contain pyrochlore as a

0003–004X/92/0102–0179$02.00

Table 1. Localities, mineral associations, and descriptions of microlite specimens

Sample nos.	Locality and lithologic unit	Alteration pattern and mineral association	I/I_0*
080, 130	Rutherford pegmatite, Amelia, VA, second intermediate zone	Crystals 1–2 cm with secondary alteration along microfractures; Ab + Qtz + Cbt ± Fgn ± Mzt ± Ryn	0.05–0.12
185	Tin Mountain pegmatite, Custer, SD, quartz-spodumene-mica zone	Crystals 0.4–1.0 mm, heavily microfractured, complete secondary alteration; Lp + Qtz ± Ms	0.00
188	Volta Grande, Minas Gerais, Brazil	Crystals 4–6 mm with thin, pink secondary alteration rinds; Wgn + Qtz ± Cbt	0.20–0.60
202	Brown Derby pegmatite, Gunnison County, CO, lepidolite-quartz zone	Crystals 0.6–1.0 mm with secondary alteration along fractures; Lp + Ms + Qtz	0.00
231	Opportunity pegmatite, Gunnison County, CO, quartz zone	Crystals 3–5 mm with secondary alteration along fractures; Qtz ± Ms	0.03
324	Pidlite pegmatite, Mora County, NM, lepidolite-quartz zone	Crystals 1–2 mm with primary alteration as uniform rims; Qtz + Lp ± Zrc ± Cbt	0.20–0.70
327	Fungwe district, Zimbabwe	A crystal 1 × 1 × 2 cm, with patchy, primary alteration; mineral association unknown	0.90–1.00
153, 260, P5.1	Harding pegmatite, Taos County, NM, cleavelandite unit	Crystals 1–6 mm with primary alteration as irregular rims, minor secondary alteration along fractures; Ab + Qtz + Ms ± Mc ± Lp ± goethite	0.00–0.15
154, 264, 269, P15.1, P17.1, P18.1	Harding pegmatite, Taos County, NM, microcline-spodumene zone	Crystals 0.5–6.0 mm with primary alteration as irregular rims and patches, minor secondary alteration along microfractures; Mc + Qtz + Spd + Ms ± Lp ± Ab ± Zrc ± goethite	0.00
P2.1, P2.2, P7.1	Harding pegmatite, Taos County, NM, lepidolite-cleavelandite subunit	Crystals 0.5–2.0 mm with primary alteration as irregular rims, minor secondary alteration along microfractures; Lp + Ab + Ms + Qtz ± Ryn ± goethite	—

* I/I_0 ranges from 0.00 for fully metamict samples to 1.00 for highly crystalline samples. All samples from the UNM collection except for 080 (USNM 96739), 185 (AMNH 34311), 188 (AMNH 24560) and 202 (HU 106185). Ab—albite, Cbt—columbite, Fgn—fergusonite, Lp—lepidolite, Mc—microcline, Ms—muscovite, Mzt—monazite, Qtz—quartz, Ryn—rynersonite or fersmite, Spm—spodumene, Wgn—wodginite, Zrc—zircon.

constituent phase (e.g., Harker, 1988; Ringwood et al., 1988).

Experimental procedures

Electron microprobe analysis

Analyses were performed using a JEOL 733 Superprobe operated at 15 kV and 20 nA with a probe diameter of 10 μm. Data were corrected for drift and dead time and then reduced using an empirical α-factor approach (Bence and Albee, 1968; Albee and Ray, 1970). Each element was counted for 40 s or until a standard deviation of 0.5% was reached. The elements F, Na, Mg, Al, K, Ca, Ti, Mn, and Fe were analyzed using $K\alpha$ spectral lines. $L\alpha$ lines were employed for Sr, Y, Zr, Nb, Sn, Sb, Cs, Ba, and REEs. For the elements Ta, W, Pb, Bi, Th, and U, $M\alpha$ lines were used. Empirical overlap corrections were determined and used for peak interference problems. Minimum detection limits are typically 0.02–0.04 wt% for the oxides of Mg, Ca, Mn, Fe, Sr, Ba, Pb, Cs, and K; 0.04–0.06 wt% for the oxides of Nb, Ta, and Na; 0.06–0.08 wt% for the oxides of Ti, Zr, Sn, Al, Y, REEs, and Sb; and 0.08–0.12 wt% for the oxides of W, Bi, Th, U, and elemental F. Standards included natural microlite, manganotantalite, cassiterite, stibiotantalite, olivine, benitoite, cerussite, pollucite, anorthite, gadolinite, and synthetic $NaNbO_3$, $CaWO_4$, $SrMoO_4$, UO_2, $CaTiO_3$, $ThSiO_4$, $ZrSiO_4$, $KTaO_3$, YPO_4, and $REEPO_4$.

X-ray diffraction analysis

Powder diffraction patterns were obtained using a Scintag diffractometer operated at 40 kV and 30 mA. Patterns were recorded from 10 to 70° 2θ at 1° per minute using graphite-monochromatized Cu$K\alpha$ radiation. BaF_2 and Si were used as internal and external standards, respectively. Lattice parameters were refined by the method of least-squares (Appleman and Evans, 1973). The level of radiation damage (I/I_0) was estimated from the total integrated intensity of all diffraction lines in the pattern relative to highly crystalline standards. Metamict and altered specimens were heated in air or N_2 for 1 h at 1000 °C and reanalyzed.

Transmission electron microscopy

Powders of selected samples were dispersed in acetone and deposited on holey-carbon filmed Cu grids. Samples were examined using a JEOL 2000FX transmission electron microscope (TEM) operated at 200 kV. High-resolution images were taken at a magnification of 410 000 using axial illumination and objective lens defocus values of −60 to −150 nm. A Tracor-Northern TN-5500 energy dispersive X-ray analyzer (EDS) was used to obtain analyses of specific areas. Spectra were acquired for 300 s real time (20–30% dead time) using an effective probe diameter of 10 nm. Data reduction was accomplished using the Tracor software package SMTF with empirical k factors determined from standards.

Criteria for recognition of alteration

Three basic criteria were used to differentiate between primary and secondary alteration: field relationships, microscopic observations, and alteration mechanisms. The first two criteria involve the use of mineral assemblages as a guide for the identification of hydrothermal alteration and weathering. In granitic pegmatites, primary

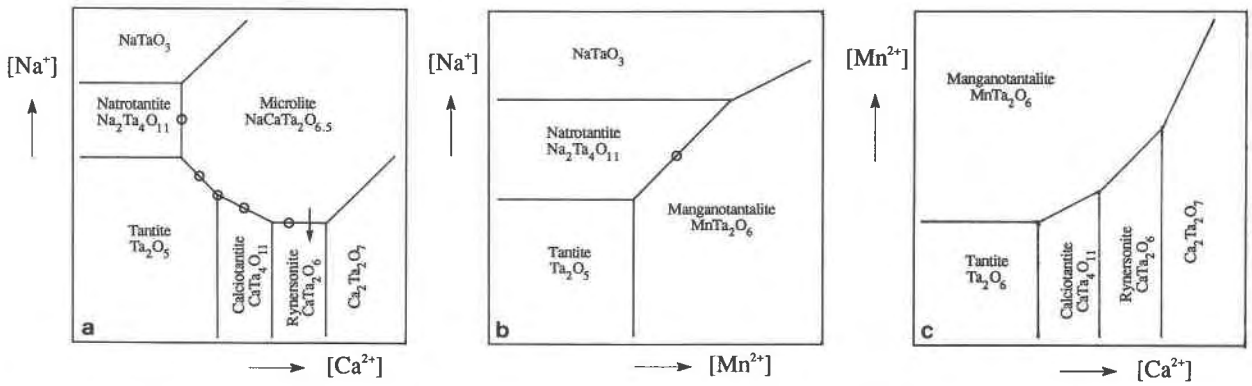

Fig. 1. Qualitative activity diagrams for the system Na-Ca-Mn-Ta-O-H based on known mineral parageneses and idealized reactions listed in Table 2. (**a**) Na-Ca, (**b**) Na-Mn, and (**c**) Mn-Ca sections. Known associations are indicated by circles, replacement features by arrows.

(hydrothermal) alteration is commonly indicated by replacement of earlier mineral assemblages by albite and lithium mica (Jahns, 1982; Hawthorne and Černý, 1982; Černý and Burt, 1984). Secondary alteration is indicated by the breakdown of feldspars and micas to clay minerals, a process often associated with the formation of iron oxyhydroxides like goethite.

Alteration mechanisms include intracrystalline diffusion and fluid transport through preexisting cracks and voids. Diffusion is an effective mechanism at high temperatures and is expected to be the dominant process during primary alteration. Fluid transport through cracks and voids with limited intracrystalline diffusion is probably the dominant mechanism operative at the relatively low temperatures characteristic of secondary alteration. The timing of alteration may be estimated where clear cross-cutting relationships with radiation-induced microfracturing exist (Lumpkin and Ewing, 1985).

The above criteria were used to classify alteration in 20 specimens (Table 1). Typical examples of primary alteration are specimens from the Harding, Pidlite, and Zimbabwe pegmatites. Alteration patterns in these microlite samples are characterized by irregular rim diffusion, uniform rim diffusion, or a patchy interior distribution, respectively. Primary alteration appears to predate most of the radiation-induced microfracturing. The best examples of secondary alteration occur in microlite samples from Amelia, Virginia, in which alteration is localized along radiation-induced microfractures with limited intracrystalline diffusion. Individual microlite crystals in sample 185 from the Tin Mountain pegmatite, South Dakota, are heavily microfractured and completely altered. Alteration was classified as secondary (see Table 1) on the basis of small crystal size, density of microfracturing, and proximity to a 1-cm layer of kaolinite in the quartz-spodumene-mica core of the pegmatite (Spilde and Shearer, 1987).

Investigation of the samples listed in Table 1 by optical microscopy, X-ray diffraction, and TEM shows that most have received extensive radiation damage. In many samples the structure has been rendered completely aperiodic (metamict) as the result of cumulative α-decay events (Lumpkin and Ewing, 1988). This study has failed to reveal conclusive evidence for natural recrystallization of chemically altered, metamict microlite. Recrystallization effects appear to be more common in radiation-damaged silicate minerals and have been observed, for example, in altered thorite group minerals from the Harding pegmatite (Lumpkin and Chakoumakos, 1988).

Tantalum oxide mineral reactions

Based on our observations of oxide mineral associations in the granitic pegmatites of northern New Mexico and Amelia, Virginia, together with those of previous investigators (e.g., von Knorring and Fadipe, 1981; Foord, 1982; Černý and Ercit, 1985, 1989; Ercit, 1986), we present here a summary of some possible reactions between microlite and other tantalum oxide minerals. Results are confined to idealized phase relations in the system Na-Ca-Mn-Ta-O-H. This system is represented by the common association of microlite, manganotantalite, fersmite, and rynersonite-vigezzite. Exotic associations reviewed by Černý and Ercit (1985, 1989) include tantite (Ta_2O_5), calciotantite ($CaTa_4O_{11}$), and natrotantite ($Na_2Ta_4O_{11}$).

In Figure 1 we have constructed schematic phase relations as a function of the activities of Na^+, Ca^{2+}, and Mn^{2+} based on idealized compositions, including $NaTaO_3$ and $Ca_2Ta_2O_7$. For simplicity, solid solution among microlite ($NaCaTa_2O_{6.5}$), rynersonite ($CaTa_2O_6$), and $Ca_2Ta_2O_7$ has been omitted. Our aim is to illustrate qualitatively how changes in fluid composition affect tantalum oxide mineral assemblages. Simple mineral reactions were used (Table 2), guided by known mineral associations or replacement features, to arrive at the topologies shown in Figure 1. For example, Figure 1a shows how the assemblages microlite + calciotantite + tantite, microlite + natrotantite, microlite + calciotantite, and microlite + rynersonite constrain the topology of the diagram.

The relations shown in Figures 1a–1c were combined

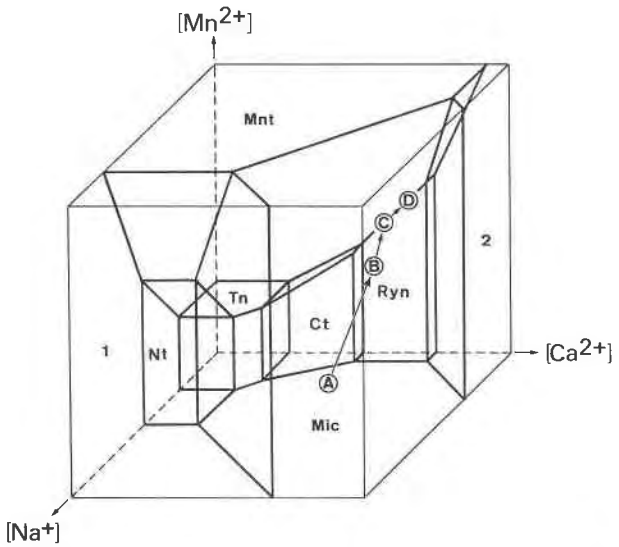

Fig. 2. Three-dimensional activity relations derived from the sections shown in Figure 1. Hypothetical reaction path A-B-C-D depicts the interaction of microlite with a fluid characterized by increasing Ca^{2+} and Mn^{2+} and decreasing Na^+ activities. Abbreviations: Ct = calciotantite, Mic = microlite, Mnt = manganotantalite, Nt = natrotantite, Ryn = rynersonite, Tn = tantite, 1 = $NaTaO_3$, 2 = $Ca_2Ta_2O_7$.

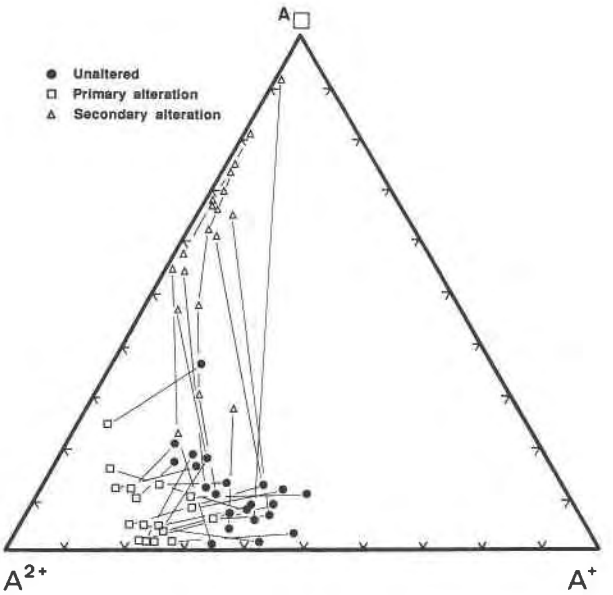

Fig. 3. Triangular plot of divalent A-site cations (mainly Ca), monovalent A-site cations (mainly Na), and A-site vacancies in unaltered and altered microlite samples.

to provide a three-dimensional view of mineral compatibility in the Na-Ca-Mn-Ta-O-H system. Figure 2 indicates that microlite and manganotantalite may coexist over a range of fluid compositions characterized by moderate to high a_{Na^+}, $a_{Ca^{2+}}$, and $a_{Mn^{2+}}$. The actual stability field of microlite may be extended by incorporation of $CaTa_2O_6$ and $Ca_2Ta_2O_7$ components in solid solution (cf. Lumpkin et al., 1986).

A hypothetical example of the breakdown of microlite is shown in Figure 2. Microlite initially in equilibrium with a fluid at point A is exposed to a fluid whose composition is characterized by increasing $a_{Ca^{2+}}$ and $a_{Mn^{2+}}$ and by decreasing a_{Na^+}. At point B, rynersonite begins to form by reaction of microlite with the fluid (Table 2, Reaction 9). Manganotantalite begins to crystallize at point C by another reaction (Table 2, Reaction 18). These three phases coexist and finally equilibrate with the fluid at point D. For a_{Na^+} values below that of point D, microlite will be completely replaced by rynersonite + manganotantalite.

TABLE 2. Mineral reactions in the system Na-Ca-Mn-Ta-O-H

1. $0.5H_2O + Ca^{2+} + 2NaTaO_3 = NaCaTa_2O_{6.5} + Na^+ + H^+$
2. $2H^+ + 4NaTaO_3 = Na_2Ta_4O_{11} + 2Na^+ + H_2O$
3. $2H_2O + 2Ca^{2+} + Na_2Ta_4O_{11} = 2NaCaTa_2O_{6.5} + 4H^+$
4. $2H^+ + Na_2Ta_4O_{11} = 2Ta_2O_5 + 2Na^+ + H_2O$
5. $1.5H_2O + Na^+ + Ca^{2+} + Ta_2O_5 = NaCaTa_2O_{6.5} + 3H^+$
6. $H_2O + Ca^{2+} + 2Ta_2O_5 = CaTa_4O_{11} + 2H^+$
7. $2H_2O + 2Na^+ + Ca^{2+} + CaTa_4O_{11} = 2NaCaTa_2O_{6.5} + 4H^+$
8. $H_2O + Ca^{2+} + CaTa_4O_{11} = 2CaTa_2O_6 + 2H^+$
9. $0.5H_2O + Na^+ + CaTa_2O_6 = NaCaTa_2O_{6.5} + H^+$
10. $H_2O + Ca^{2+} + CaTa_2O_6 = Ca_2Ta_2O_7 + 2H^+$
11. $H^+ + Na^+ + Ca_2Ta_2O_7 = NaCaTa_2O_{6.5} + Ca^{2+} + 0.5H_2O$
12. $Mn^{2+} + 2NaTaO_3 = MnTa_2O_6 + 2Na^+$
13. $H_2O + 2Mn^{2+} + Na_2Ta_4O_{11} = 2MnTa_2O_6 + 2Na^+ + 2H^+$
14. $H_2O + Mn^{2+} + Ta_2O_5 = MnTa_2O_6 + 2H^+$
15. $2H^+ + Mn^{2+} + Ca_2Ta_2O_7 = MnTa_2O_6 + 2Ca^{2+} + H_2O$
16. $Mn^{2+} + CaTa_2O_6 = MnTa_2O_6 + Ca^{2+}$
17. $H_2O + 2Mn^{2+} + CaTa_4O_{11} = 2MnTa_2O_6 + Ca^{2+} + 2H^+$
18. $0.5H_2O + Na^+ + Ca^{2+} + MnTa_2O_6 = NaCaTa_2O_{6.5} + Mn^{2+} + H^+$

Note: $NaCaTa_2O_{6.5}$ = microlite, $MnTa_2O_6$ = manganotantalite, $CaTa_4O_{11}$ = calciotantite, $CaTa_2O_6$ = rynersonite or fersmite, $Na_2Ta_4O_{11}$ = natrotantite, Ta_2O_5 = tantite.

Chemical effects of alteration

Primary alteration

Electron microprobe analyses of microlite samples from the Harding pegmatite (Tables 3 and 4[1]) demonstrate that the major chemical effects of primary alteration are decreased Na and increased Ca, Fe, Mn, and O. The amounts of U, F, and inferred H_2O (estimated by difference) tend to remain relatively constant, although lower F and higher inferred H_2O contents were noted in a few samples. Similar results were found in sample 324 from the Pidlite pegmatite, Mora County, New Mexico, and in sample 327 from the Fungwe district, Zimbabwe. Structural formulas of sample 324 indicate that Ca, Mn, Fe, and O increased and that Na, $^A\square$, and $^Y\square$ decreased as a result of alteration. For sample 327, structural formulas clearly indicate strong Ca enrichment and Na depletion during primary alteration. Following a typical pattern, the amount of O increased in the altered areas, whereas $^A\square$ and $^Y\square$ decreased. The Mn content and inferred H_2O remained constant, but Fe decreased during alteration.

[1] To receive a copy of Table 4, order Document AM-92-488 from the Business Office, Mineralogical Society of America, 1130 Seventeenth Street NW, Suite 330, Washington, DC 20036, U.S.A. Please remit $5.00 in advance for the microfiche.

TABLE 3. Representative electron microprobe analyses of unaltered and altered areas of six microlite samples

	130	130s	202	202s	188	188s	231	231s	324	324p	327	327p
WO_3	0.43	0.28	0.06	0.16	0.10	0.31	0.31	0.51	0.12	0.00	0.04	0.00
Nb_2O_5	10.6	11.5	9.24	9.21	2.03	2.05	3.82	3.91	14.3	14.4	6.15	5.20
Ta_2O_5	62.0	64.5	58.9	61.6	76.3	72.7	71.1	71.6	61.9	60.3	76.5	76.1
TiO_2	1.10	1.10	0.03	0.04	0.04	0.14	0.17	0.16	0.11	0.10	1.35	1.06
SnO_2	2.01	2.28	2.41	2.19	1.75	2.28	0.46	0.76	0.12	0.16	0.26	0.28
ThO_2	0.20	0.09	0.00	0.00	0.00	0.00	0.01	0.00	0.12	0.15	0.00	0.00
UO_2	1.57	1.28	9.28	8.74	2.22	3.20	3.85	4.24	3.25	3.29	0.00	0.00
Al_2O_3	0.04	0.06	0.00	0.00	0.08	0.20	0.00	0.00	0.09	0.08	0.01	0.01
Y_2O_3	0.15	0.20	0.06	0.07	0.03	0.18	0.07	0.09	0.09	0.09	0.05	0.00
REE_2O_3	0.14	0.25	0.26	0.11	0.30	0.80	0.10	0.20	0.14	0.17	0.10	0.14
Sb_2O_3	0.00	0.03	0.08	0.14	0.00	0.06	0.46	0.30	0.06	0.12	0.07	0.13
Bi_2O_3	0.00	0.00	0.04	0.08	0.00	0.00	0.01	0.00	0.04	0.08	0.10	0.11
CaO	12.6	5.83	10.0	8.14	11.2	0.01	10.9	8.57	12.4	14.8	11.2	16.0
MnO	0.00	0.17	0.20	0.00	0.11	0.00	0.30	0.47	0.10	0.49	0.15	0.18
FeO	0.06	0.58	0.52	0.13	0.03	0.83	0.56	0.25	0.00	0.49	0.12	0.02
BaO	0.00	0.00	0.00	0.00	0.00	4.00	0.05	0.05	0.00	0.00	0.03	0.00
PbO	0.22	0.19	0.20	0.40	0.01	0.21	0.13	0.23	0.29	0.16	0.00	0.01
Na_2O	3.62	0.20	4.08	0.13	4.08	0.00	3.82	2.72	2.92	1.29	1.82	0.59
Cs_2O	0.00	0.00	0.00	0.00	0.00	0.12	0.00	0.01	0.00	0.00	0.00	0.00
F	2.7	0.12	2.1	1.6	2.4	0.01	2.6	1.2	1.5	1.2	1.3	1.3
Sum	97.44	88.66	97.46	92.74	100.68	87.10	98.72	95.27	97.55	97.35	99.47	101.25
O ≡ F	−1.13	−0.05	−0.88	−0.67	−1.01	−0.00	−1.09	−0.50	−0.63	−0.50	−0.55	−0.55
Total	96.31	88.61	96.58	92.07	99.67	87.10	97.63	94.77	96.92	96.85	98.92	100.70
					Structural formulas based on Σ B = 2.00							
W	0.010	0.006	0.002	0.004	0.002	0.002	0.007	0.012	0.003	0.000	0.001	0.000
Nb	0.409	0.422	0.391	0.381	0.081	0.098	0.161	0.162	0.548	0.562	0.225	0.196
Ta	1.439	1.425	1.499	1.533	1.843	1.817	1.803	1.787	1.429	1.417	1.683	1.726
Ti	0.071	0.067	0.002	0.003	0.003	0.009	0.012	0.011	0.007	0.007	0.082	0.066
Sn	0.068	0.074	0.089	0.080	0.062	0.051	0.017	0.028	0.004	0.006	0.008	0.009
Al	0.004	0.006	0.000	0.000	0.008	0.023	0.000	0.000	0.009	0.008	0.001	0.001
Fe^{3+}	0.000	0.000	0.017	0.000	0.000	0.000	0.000	0.000	0.000	0.000	0.000	0.000
Th	0.004	0.002	0.000	0.000	0.000	0.002	0.000	0.000	0.002	0.003	0.000	0.000
U	0.030	0.023	0.193	0.178	0.044	0.027	0.080	0.087	0.061	0.063	0.000	0.000
Y	0.007	0.009	0.003	0.003	0.001	0.010	0.003	0.004	0.004	0.004	0.002	0.000
REE	0.004	0.007	0.009	0.004	0.010	0.020	0.003	0.007	0.004	0.005	0.003	0.004
Sb	0.000	0.001	0.003	0.005	0.000	0.008	0.018	0.011	0.002	0.004	0.002	0.001
Bi	0.000	0.000	0.001	0.002	0.000	0.000	0.000	0.000	0.001	0.002	0.002	0.002
Ca	1.152	0.507	1.002	0.798	1.066	0.002	1.089	0.843	1.128	1.370	0.971	1.430
Mn	0.000	0.012	0.016	0.000	0.008	0.001	0.024	0.037	0.007	0.036	0.010	0.013
Fe^{2+}	0.004	0.039	0.025	0.010	0.002	0.007	0.044	0.019	0.000	0.035	0.008	0.001
Ba	0.000	0.000	0.000	0.000	0.000	0.112	0.002	0.002	0.000	0.000	0.001	0.000
Pb	0.005	0.004	0.007	0.010	0.000	0.039	0.003	0.006	0.007	0.004	0.000	0.000
Na	0.599	0.032	0.741	0.023	0.702	0.002	0.690	0.484	0.480	0.216	0.285	0.095
Σ A	1.805	0.636	2.000	1.033	1.834	0.288	1.956	1.499	1.697	1.744	1.285	1.547
O	6.111	5.565	6.412	5.940	6.158	5.215	6.289	6.170	6.318	6.532	5.930	6.288
F	0.729	0.031	0.624	0.454	0.669	0.011	0.746	0.343	0.389	0.328	0.343	0.350
Σ (X + Y)	6.841	5.596	7.036	6.395	6.827	5.226	7.035	6.513	6.707	6.860	6.273	6.638

Note: A letter at the end of a sample number indicates alteration: s = secondary, p = primary. Mg, K, Sr, and Zr were below detection limits and are not reported. All Fe allocated to the A site except for analyses with Σ A > 2.00, for which enough Fe was allocated to the B site to give Σ A = 2.00.

A triangular plot of A-site cations and vacancies (Fig. 3) demonstrates the consistent increase in divalent cations during primary alteration. Monovalent cations (essentially Na) usually decrease but in a few cases remain relatively constant. A-site vacancies tend to decrease or remain relatively constant. Two samples showed minor increases in the number of A-site vacancies. A similar plot of anions and vacancies (Fig. 4) indicates that O increases, F tends to decrease or remain relatively constant, and anion vacancies usually decrease. The U contents of altered areas remain unchanged in comparison to unaltered areas (Fig. 5). Apart from Pb, which shows minor decreases in some samples, the divalent cations Ca, Mn, and Fe generally increase during alteration. Average increases in these cations are approximately 0.25 Ca, 0.05 Mn, and 0.03 Fe atoms per formula unit (Fig. 6). Major substitutions inferred from these results are $^{A}\square^{Y}\square \rightarrow {}^{A}Ca^{Y}O$, $^{A}Na^{Y}F \rightarrow {}^{A}Ca^{Y}O$, and $^{A}Na^{Y}OH \rightarrow {}^{A}Ca^{Y}O$. The latter substitution is postulated for the cases where F remains relatively constant and O increases. The simple substitution $^{Y}F \rightarrow {}^{Y}OH$ is also possible but is largely masked by coupled substitutions.

The substitutions noted above can be related to pervasive, subsolidus alteration by exchange reactions of the form:

$$H_2O + Ca^{2+} + [CaTa_2O_6]_{mss} = [Ca_2Ta_2O_7]_{mss} + 2H^+ \quad (19)$$

$$H_2O + Ca^{2+} + [NaCaTa_2O_6F]_{mss} = [Ca_2Ta_2O_7]_{mss} + Na^+ + H^+ + HF \quad (20a)$$

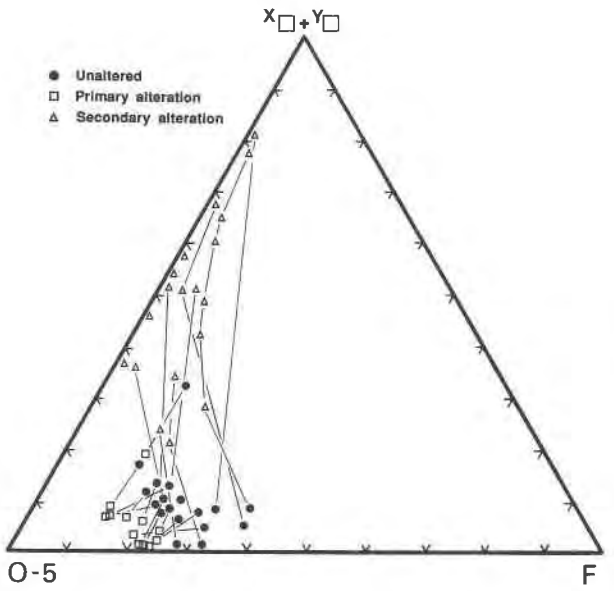

Fig. 4. Triangular plot of X- and Y-site anions and vacancies in unaltered and altered microlite samples. The O content is plotted as O-5 to give the same scale as in Figure 3.

$$Ca^{2+} + [NaCaTa_2O_6OH]_{mss} = [Ca_2Ta_2O_7]_{mss} + Na^+ + H^+ \quad (20b)$$

$$0.5H_2O + Ca^{2+} + [NaCaTa_2O_{6.5}]_{mss} = [Ca_2Ta_2O_7]_{mss} + Na^+ + H^+. \quad (20c)$$

Reaction 20 is given in three forms to account for occupancy of the Y site by F, O, or OH. The right side of each reaction is favored by relatively high $a_{Ca^{2+}}$ and pH and by low a_{Na^+} in the fluid phase. Equations 19, 20a, and 20c indicate that temperature and the activities of H_2O and HF also play a role in controlling the composition of microlite. In situations where F remains relatively constant, Reactions 20b and 20c best account for chemical changes attending primary alteration.

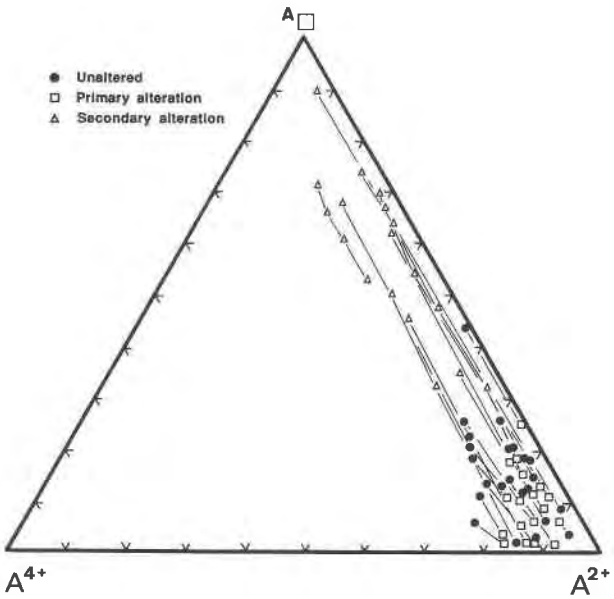

Fig. 5. Triangular plot of tetravalent A-site cations (mainly U), divalent A-site cations (mainly Ca), and A-site vacancies in unaltered and altered microlite samples.

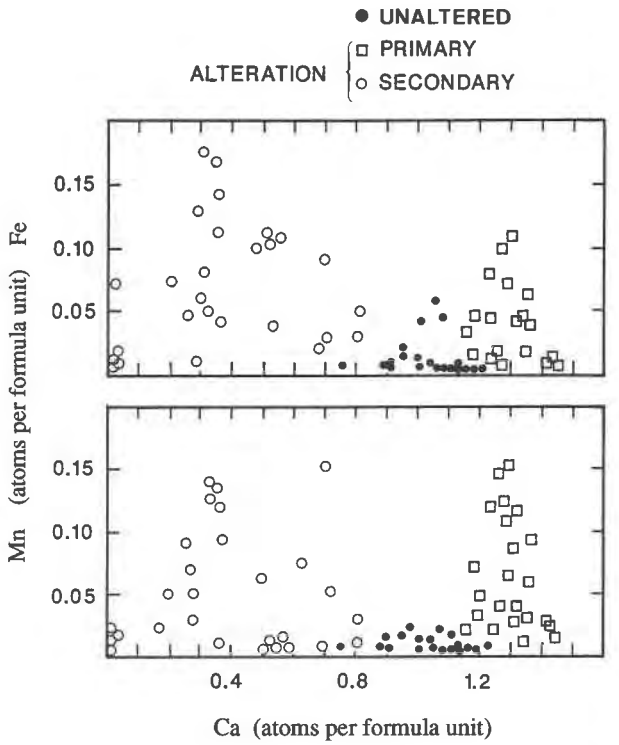

Fig. 6. Plots of Mn and Fe vs. Ca in unaltered and altered microlite samples.

Secondary alteration

Examination of Figure 3 shows that alteration causes compositions to move toward the $^{A}\square$-A^{2+} join as Na is removed at a faster rate than divalent cations. Among the divalent cations, Figure 6 shows that Ca is lost, whereas Mn and Fe usually show slight to moderate gains (up to 0.15 atoms per formula unit). Minor increases in Pb also occur in some specimens. With the exception of sample 188, Ba shows slight increases in only a few of the microlite samples. Once Na is completely leached from the A site, compositions then move toward the $^{A}\square$ vertex of Figure 3 as Ca continues to be removed. In sample 080, the compositions plot along a curved trend, indicating a gradual increase in the relative rate of Ca loss with progressive alteration.

Alteration trends represented by the anions (Fig. 4) closely follow those of the cations (Fig. 3). Figure 4 shows that, initially, F is removed from the Y site, causing compositions to move toward the ($^{X}\square + {}^{Y}\square$)–(O-5) join. As alteration proceeds, O is removed from the X and Y sites, causing compositions to approach the $^{X}\square + {}^{Y}\square$ vertex of

Figure 4. Notice in Figure 4 that data for sample 080 follow a curved path complementary to the cation trend shown in Figure 3.

Combined results for cations and anions indicate that Schottky defects are produced by substitutions of the form $^{A}Na^{Y}F \rightarrow {}^{A}\square^{Y}\square$, $^{A}Ca^{Y}O \rightarrow {}^{A}\square^{Y}\square$, and $^{A}Ca^{X}O \rightarrow {}^{A}\square^{X}\square$. Simple substitutions such as $^{Y}F \rightarrow {}^{Y}OH$ and $^{A}Ca^{2+} \rightarrow 2H^{+}$ are possible but tend to be masked by coupled substitutions. Also, structural considerations indicate that only minor amounts of OH^{-} will be tolerated at the Y site in conjuction with large numbers of cation vacancies (Subramanian et al., 1983). The major substitutions result in highly defective, hydrated microlite samples characterized by increases of 4 to 13 wt% H_2O. Furthermore, Figure 5 shows that the U content of microlite remains remarkably constant as a result of secondary alteration.

In most samples, vacancies reach maximum values of $^{A}\square = 1.5$, $^{Y}\square = 1.0$, and $^{X}\square = 0.5$ per formula unit (Tables 3 and 4). Sample 188 from Minas Gerais, Brazil, consists of crystals of unaltered microlite with thin alteration rinds of bariomicrolite in which vacancies reach maximum values of $^{A}\square = 1.8$, $^{Y}\square = 1.0$, and $^{X}\square = 0.8$ per formula unit. Structural formulas indicate virtually complete leaching of Ca, Na, and F, compensated in part by entry of minor amounts of Ba, Pb, Fe, REEs, Cs, and 10–12 wt% H_2O.

Secondary alteration, or weathering, of microlite can be approximated by reactions of the form:

$$3H^{+} + H_2O + [NaCaTa_2O_6F]_{mss} = [Ta_2O_5 \cdot 2H_2O]_{mss} + Na^{+} + Ca^{2+} + HF \quad (21)$$

$$2H^{+} + 1.5H_2O + 0.5Ba^{2+} + [NaCaTa_2O_6F]_{mss} = [Ba_{0.5}Ta_2O_{5.5} \cdot 2H_2O]_{mss} + Na^{+} + Ca^{2+} + HF. \quad (22)$$

The right side of each reaction is favored by relatively low T, low pH, and low a_{Na^+}, $a_{Ca^{2+}}$, and a_{HF} in the fluid phase. Additionally, Reaction 22 is favored by relatively high $a_{Ba^{2+}}$ in solution.

U-Pb systematics

Microprobe analyses were used to evaluate the behavior of U and Pb in microlite subsequent to crystallization. The Harding suite was selected because a large number of samples are available, the geologic age is well established at 1300 m.y. (Aldrich et al., 1958; Brookins et al., 1979), significant metamorphic overprinting is absent, and the microlite samples have low Th and high U contents (Lumpkin et al., 1986). Figure 7 shows a U-Pb plot including both unaltered and altered microlite samples from the Harding pegmatite. Most of the data fall below the 1300-m.y. reference line. Except for specific examples, the magnitude of Pb loss is poorly correlated with alteration. The maximum degree of Pb loss approaches 80% in both unaltered and altered material, suggesting that long-term diffusion is a viable explanation of the results. The high-Pb data points in Figure 7 are from the core of a microlite grain in sample 269 and represent either Pb gain during alteration or common Pb incorporated during crystallization.

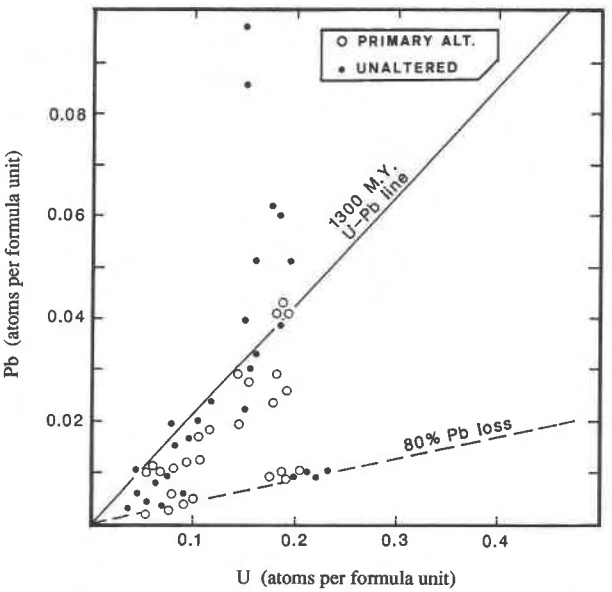

Fig. 7. U-Pb systematics of unaltered and altered microlite samples.

Data for microlite samples from other approximately 1300-m.y.-old pegmatites are generally consistent with the Harding suite. Microlite crystals from the Pidlite pegmatite exhibit Pb loss of 0–35% in unaltered cores and 60–75% in altered rims. These results are consistent with either episodic Pb loss during primary alteration or a subsequent long-term diffusion gradient preserved over a distance of 0.5–1.0 mm from core to rim. In comparison, heavily microfractured microlite crystals (samples 202 and 231) from the Quartz Creek district, Colorado, consistently show 60–80% Pb loss in both unaltered and altered areas. In this case the alteration is classified as secondary (Table 1). The U-Pb systematics reported above indicate that radiation-induced microfracturing plays an important role in controlling the long-term loss of radiogenic Pb in microlite.

Discussion

Chemical effects of alteration

Chemical changes that accompany alteration are summarized in Figure 8 using idealized end-members to show major element trends. Most unaltered compositions fall near the $NaCaTa_2O_6F$-$CaTa_2O_6$ join or just within the $NaCaTa_2O_6F$-$Ca_2Ta_2O_7$-$CaTa_2O_6$ composition field. Four alteration vectors are indicated by the data in Figures 3 and 4: (1) filling of Schottky defects by CaO, (2) NaF → CaO exchange, (3) formation of Schottky defects by removal of NaF, and (4) creation of Schottky defects by removal of CaO. Although there are obvious differences between individual samples, primary alteration paths lie consistently between trends 1 and 2 (Fig. 8).

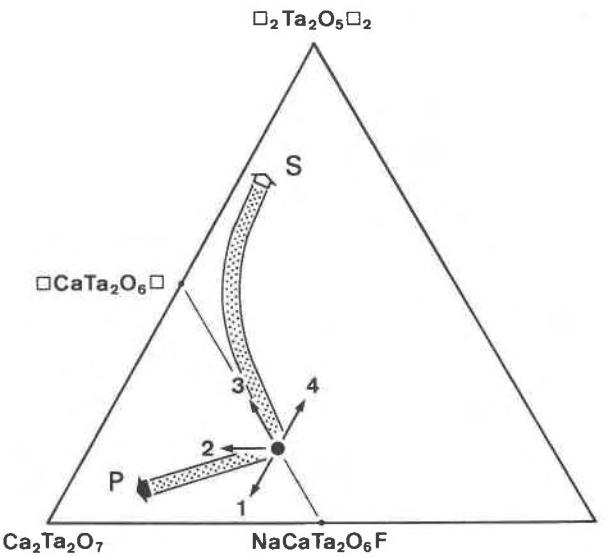

Fig. 8. Ternary plot summarizing the major element trends for primary (P) and secondary (S) alteration of microlite. Vectors 1–4 are described in the text.

Secondary alteration follows a distinctly different path between trends 3 and 4, gradually approaching trend 4 as alteration proceeds to completion. In cases of extreme secondary alteration, this path ultimately requires that some O be removed from the X site. The occurrence of paired vacancies (Schottky defects) is consistent with the geometry of the pyrochlore structure type, in which YA_4 tetrahedra and AX_6Y_2 distorted cubic sites exist within large cavities of a stable B_2X_6 octahedral framework (Subramanian et al., 1983; Chakoumakos, 1984). These large cavities are interconnected in three dimensions by channels, through which A- and Y-site ions can be removed in combinations that maintain overall charge balance.

Microlite also commonly exhibits slight to moderate increases in Mn and Fe during primary or secondary alteration. In the Harding microlite samples, values of Σ A > 2.00 atoms per formula unit require that essentially all of the Fe and part of the Mn incorporated during primary alteration to be located at the B site as Fe^{3+} and Mn^{3+} (Lumpkin et al., 1986). During secondary alteration, microlite may exhibit slight to moderate increases in the Ba content. A slight increase in Cs was noted in the bariomicrolite sample from Brazil.

The exceptional stability of U in the A site results in part from the coordination geometry, where true leaching is restricted to cations of low formal valence. Removal of a U^{4+} or U^{6+} ion would be difficult to charge balance in combination with Y-site anions alone. Long-term loss of radiogenic Pb in microlite is supported by the work of Aldrich et al. (1958), who found that microlite samples from the Harding pegmatite give discordant U-Pb ages. The authors investigated two samples, one with 0.7 wt% U and 0.1 wt% Pb and another with 7.7 wt% U and 1.1 wt% Pb. Both gave ^{238}U-^{206}Pb and ^{235}U-^{207}Pb isotopic ages of 900–1000 m.y., consistent with loss of 20–30% of the radiogenic Pb.

Conditions of alteration

Members of the microlite subgroup show well-defined primary and secondary alteration in terms of both textural and chemical features. We suggest that this is related to the depth of emplacement of the host rocks. Most granitic pegmatites of the rare-element class are emplaced at depths of 4–12 km (Jahns, 1982; London, 1984; Černý, 1989; Chakoumakos and Lumpkin, 1990; Norton and Redden, 1990). Becaue of the small size of granitic pegmatites, the cooling rate is rapid in comparison with much larger granitic plutons. On the basis of cooling models for a finite slab with dimensions of 2 × 2 × 0.02 km, Chakoumakos and Lumpkin (1990) estimated that the magmatic phase of the Harding pegmatite lasted only 100–1000 yr. Emplacement at relatively deep crustal levels means that subsequent hydrothermal activity will usually have ended long before granitic pegmatites reach the surface following uplift and erosion.

Primary alteration of microlite occurred during the late magmatic to hydrothermal stages of pegmatite emplacement at $P = 2$–4 kbar and $T = 350$–550 °C (cf. Chakoumakos and Lumpkin, 1990). Alteration is influenced by the presence and evolution of a dense silicate liquid and supercritical H_2O-CO_2-$NaCl_{eq}$ fluid rich in volatiles and fluxing elements such as F, Li, Be, B, P, Rb, and Cs (Jahns, 1982; London, 1986, 1987; Černý, 1989). Exchange reactions between microlite and fluid suggest conditions of relatively high pH, high $a_{Ca^{2+}}$, and low a_{Na^+}, often accompanied by elevated $a_{Mn^{2+}}$ and $a_{Fe^{2+}}$. The requirement of Fe^{3+} and Mn^{3+} to occupy the B site in some of the Harding microlite samples suggests that relatively high f_{O_2} conditions prevailed during alteration. This is supported by high U^{6+}/U^{4+} ratios in microlite (Jahns and Ewing, 1976) and the incorporation of V^{5+} and Bi^{3+} in thorite during primary alteration (Lumpkin and Chakoumakos, 1988). Modeling of mineral reactions in the system Na-Ca-Mn-Ta-O-H indicates that if the increases in $a_{Ca^{2+}}$ and $a_{Mn^{2+}}$ proceed far enough, microlite will be replaced by rynersonite (or fersmite) and manganotantalite.

Secondary alteration is characteristic of near-surface conditions with $T < 100$ °C and $P < 1$ kbar. Alteration occurs in the presence of relatively large volumes of meteoric H_2O and is mainly controlled by radiation-induced microfractures. Exchange reactions between microlite and meteoric H_2O suggest conditions of relatively low a_{Na^+}, $a_{Ca^{2+}}$, a_{HF}, and pH, resulting in leaching of Na, Ca, F, and O accompanied by hydration. In special circumstances, cations like Cs, Ba, or Pb may be picked up by meteoric H_2O through dissolution of unstable silicate minerals and subsequently exchanged with microlite during secondary alteration.

Conclusions

This investigation shows that the microlite subgroup is a useful indicator of geochemical processes occurring at hydrothermal temperatures during the latter stages of pegmatite emplacement. Relative changes in fluid composition can be assessed through the use of tantalum oxide mineral associations, replacement reactions, intracrystalline zoning patterns, and subsequent primary alteration effects.

Results of this study are also relevant to nuclear waste disposal using ceramic waste forms and show that pyrochlore structure types are susceptible to leaching of cations and anions at low temperatures. This effect may be enhanced by prior radiation damage and microfracturing. The next two papers in this series will address alteration effects in the pyrochlore and betafite subgroups, encompassing a broader range of compositions and geologic environments, including carbonatites and nepheline syenite pegmatites.

Acknowledgments

We thank Carl Francis of Harvard University, John White, Jr. of the Smithsonian Institution, and George Harlow of the American Museum of Natural History for providing some of the samples. Much of this work is based on the collection of microlite samples from the Harding pegmatite at the University of New Mexico, for which we acknowledge the efforts of Art Montgomery, B.C. Chakoumakos, and all those involved in preserving this remarkable locality. We thank E.R. Vance, T.J. White, and an anonymous referee for providing critical reviews of this manuscript. Electron microprobe analyses and transmission electron microscopy were completed in the Electron Microbeam Analysis Facility in the Department of Geology and Institute of Meteoritics at the University of New Mexico, supported in part by NSF, NASA, DOE-BES, and the State of New Mexico. This work was supported by the Department of Energy, Office of Basic Energy Sciences, under grant DE-FG04-84ER45099.

References cited

Albee, A.L., and Ray, L. (1970) Correction factors for electron probe microanalysis of silicates, oxides, carbonates, phosphates, and sulfates. Analytical Chemistry, 42, 1408–1414.

Aldrich, L.T., Wetherill, G.W., Davis, G.L., and Tilton, G.R. (1958) Radioactive ages of micas from granitic rocks by Rb-Sr and K-Ar methods. Transactions of the American Geophysical Union, 39, 1124–1134.

Appleman, D.E., and Evans, H.T., Jr. (1973) Indexing and least-squares refinement of X-ray powder data. United States National Technical Information Service, Document Pb-216-188.

Bence, A.E., and Albee, A.L. (1968) Empirical correction factors for the electron microanalysis of silicates and oxides. Journal of Geology, 76, 382–403.

Brookins, D.G., Chakoumakos, B.C., Cook, C.W., Ewing, R.C., Landis, G.P., and Register, M.E. (1979) The Harding pegmatite: Summary of recent research. In R.V. Ingersoll and L.A. Woodward, Eds., New Mexico Geological Society Guidebook, 30th Field Conference, p. 127–133. New Mexico Geological Society, Socorro, New Mexico.

Černý, P. (1989) Characteristics of pegmatite deposits of tantalum. In P. Möller, P. Černý, and F. Saupé, Eds., Lanthanides, tantalum and niobium, p. 196–239. Springer-Verlag, Berlin.

Černý, P., and Burt, D.M. (1984) Paragenesis, crystallochemical characteristics and geochemical evolution of micas in granitic pegmatites. In Mineralogical Society of America Reviews in Mineralogy, 13, 257–298.

Černý, P., and Ercit, T.S. (1985) Some recent advances in the mineralogy and geochemistry of Nb and Ta in rare-element granitic pegmatites. Bulletin de Minéralogie, 108, 499–532.

——— (1989) Mineralogy of niobium and tantalum: Crystal chemical relationships, paragenetic aspects and their economic implications. In P. Möller, P. Černý, and F. Saupé, Eds., Lanthanides, tantalum and niobium, p. 27–79. Springer-Verlag, Berlin.

Chakoumakos, B.C. (1984) Systematics of the pyrochlore structure type, ideal $A_2B_2X_6Y$. Journal of Solid State Chemistry, 53, 120–129.

Chakoumakos, B.C., and Lumpkin, G.R. (1990) Pressure-temperature constraints on the crystallization of the Harding pegmatite, Taos County, New Mexico. Canadian Mineralogist, 28, 287–298.

Ercit, T.S. (1986) The simpsonite paragenesis: The crystal chemistry and geochemistry of extreme Ta fractionation. Ph.D. dissertation, University of Manitoba, Winnipeg.

Ewing, R.C. (1975) Alteration of metamict, rare-earth, AB_2O_6-type Nb-Ta-Ti oxides. Geochimica et Cosmochimica Acta, 39, 521–530.

Foord, E.E. (1982) Minerals of tin, titanium, niobium and tantalum in granitic pegmatites. In Mineralogical Association of Canada Short Course Handbook, 8, 187–238.

Groult, D., Pannetier, J., and Raveau, B. (1982) Neutron diffraction study of the defect pyrochlores $TaWO_{5.5}$, $H_2Ta_2O_6$, and $HTaWO_6 \cdot H_2O$. Journal of Solid State Chemistry, 41, 277–285.

Harker, A.B. (1988) Tailored ceramics. In W. Lutze and R.C. Ewing, Eds., Radioactive waste forms for the future, p. 335–392. North-Holland, Amsterdam.

Hawthorne, F.C., and Černý, P. (1982) The mica group. In Mineralogical Association of Canada Short Course Handbook, 8, 63–98.

Hogarth, D.D. (1977) Classification and nomenclature of the pyrochlore group. American Mineralogist, 62, 403–410.

Jahns, R.H. (1982) Internal evolution of pegmatite bodies. In Mineralogical Association of Canada Short Course Handbook, 8, 293–327.

Jahns, R.H., and Ewing, R.C. (1976) The Harding mine, Taos County, New Mexico. In R.C. Ewing and B.S. Kues, Eds., New Mexico Geological Society Guidebook, 27th Field Conference, p. 263–276. New Mexico Geological Society, Socorro, New Mexico.

London, D. (1984) Experimental phase equilibria in the system $LiAlSiO_4$-SiO_2-H_2O: A petrogenetic grid for lithium-rich pegmatites. American Mineralogist, 69, 995–1004.

——— (1986) Magmatic-hydrothermal transition in the Tanco rare-element pegmatite: Evidence from fluid inclusions and phase-equilibrium experiments. American Mineralogist, 71, 376–395.

——— (1987) Internal differentiation of rare-element pegmatites: Effects of boron, phosphorus, and fluorine. Geochimica et Cosmochimica Acta, 51, 403–420.

Lumpkin, G.R. (1989) Alpha-decay damage, geochemical alteration, and crystal chemistry of natural pyrochlores. Ph.D. dissertation, University of New Mexico, Albuquerque.

Lumpkin, G.R., and Chakoumakos, B.C. (1988) Chemistry and radiation effects of thorite-group minerals from the Harding pegmatite, Taos County, New Mexico. American Mineralogist, 73, 1405–1419.

Lumpkin, G.R., and Ewing, R.C. (1985) Natural pyrochlores: Analogues for actinide host phases in radioactive waste forms. Materials Research Society Symposium Proceedings, 44, 647–654.

——— (1988) Alpha-decay damage in minerals of the pyrochlore group. Physics and Chemistry of Minerals, 16, 2–20.

Lumpkin, G.R., Chakoumakos, B.C., and Ewing, R.C. (1986) Mineralogy and radiation effects of microlite from the Harding pegmatite, Taos County, New Mexico. American Mineralogist, 71, 569–588.

Norton, J.J., and Redden, J.A. (1990) Relations of zoned pegmatites to other pegmatites, granite, and metamorphic rocks in the southern Black Hills, South Dakota. American Mineralogist, 75, 631–655.

Ringwood, A.E., Kesson, S.E., Reeve, K.D., Levins, D.M., and Ramm, E.J. (1988) Synroc. In W. Lutze and R.C. Ewing, Eds., Radioactive waste forms for the future, p. 233–334. North-Holland, Amsterdam.

Rotella, F.J., Jorgensen, J.D., Biefeld, R.M., and Morosin, B. (1982) Location of deuterium sites in the defect pyrochlore $DTaWO_6$ from neutron powder diffraction data. Acta Crystallographica, B38, 1697–1703.

Spilde, M.N., and Shearer, C.K. (1987) A comparison of tantalum-niobium mineral assemblages in two mineralogically distinct rare-element pegmatites. Geological Society of America Abstracts with Programs, 19, 853.

Subramanian, M.A., Aravamudan, G., and Subba Rao, G.V. (1983) Oxide pyrochlores—A review. Progress in Solid State Chemistry, 15, 55–143.

Van Wambeke, L. (1970) The alteration processes of the complex titano-niobo-tantalates and their consequences. Neues Jahrbuch für Mineralogie Abhandlungen, 112, 117–149.

von Knorring, O., and Fadipe, A. (1981) On the mineralogy and geochemistry of niobium and tantalum in some granite pegmatites and alkali granites of Africa. Bulletin de Minéralogie, 104, 496–507.

Manuscript received August 9, 1990
Manuscript accepted September 11, 1991

ERRATUM

Manganese, ferric iron, and the equilibrium between garnet and biotite, by M. L. Williams and J. A. Grambling (v. 75, p. 886–908). The final term in Equations 12 and 13 should be negative. Also, the first term is slightly low due to rounding errors. The correct form of Equation 13 is

$$\begin{aligned} T(\mathrm{K}) = [&-17368 - 79.5(P) + 1579 \\ &- W_{MgFe}(X_{alm} - X_{prp}) - 12550(X_{grs}) - 8230(X_{sps})] \\ &- R[\ln K_D - 0.782 - \ln(Fe^{2+}Bt/Fe^{Tot,Bt})^*] \end{aligned} \quad (13)$$

where K_D includes only Fe^{2+} and starred terms refer to the composition of the minerals in the calibration experiments. Note that, for clarity, the final term has been maintained as in Equation 12. Also, in Table 10, W^{Gt}_{MnMg} should be changed to 7285, 20775, and 10031 for Models 1, 2, and 3, respectively.